

Cosmic Shear E/B-mode Estimation with Binned Correlation Function Data

Matthew R. Becker*

Department of Physics, 5720 S. Ellis Avenue, The University of Chicago, Chicago, IL 60637

Kavli Institute for Cosmological Physics, 5640 South Ellis Avenue, The University of Chicago, Chicago, IL 60637

ABSTRACT

In this work I study the problem of E/B-mode separation with binned cosmic shear two-point correlation function data. Motivated by previous work on E/B-mode separation with shear two-point correlation functions and the practical considerations of data analysis, I consider E/B-mode estimators which are linear combinations of the binned shear correlation function data points. I demonstrate that these estimators mix E- and B-modes generally. I then show how to define estimators which minimize this E/B-mode mixing and give practical recipes for their construction and use. Using these optimal estimators, I demonstrate that the vector space composed of the binned shear correlation function data points can be decomposed into approximately ambiguous, E- and B-mode subspaces. With simple Fisher information estimates, I show that a non-trivial amount of information on typical cosmological parameters is contained in the ambiguous mode subspace computed in this formalism. Next, I give two examples which apply these practical estimators and recipes to generic problems in cosmic shear data analysis: data compression and spatially locating B-mode contamination. In particular, by using wavelet-like estimators with the shear correlation functions directly, one can pinpoint B-mode contamination to specific angular scales and extract information on its shape. Finally, I discuss how these estimators can be used as part of blinded or closed-box cosmic shear data analyses in order to assess and find B-mode contamination at high-precision while avoiding observer biases.

Key words: gravitational lensing: weak; cosmology: theory; methods: data analysis

1 INTRODUCTION

Cosmic shear, or the weak gravitational lensing of background galaxies by cosmological density fields, is one of the most important techniques for probing the properties of Dark Energy (see, e.g., Weinberg et al. 2012 for a recent review) and also the growth of structure predicted by General Relativity (GR) or its possible modifications (e.g., Schmidt 2008; Beynon et al. 2010; Vanderveld et al. 2011). Cosmic shear measurements can also help constrain other cosmologically interesting signals, such as primordial non-Gaussianity (e.g., Fedeli & Moscardini 2010; Marian et al. 2011; Maturi et al. 2011; Giannantonio et al. 2012; Hilbert et al. 2012), the properties of various hot and warm dark matter models (e.g., Schaefer et al. 2008; Debono et al. 2010; Markovic et al. 2011), or the properties of neutrinos (e.g., Cooray 1999; Song & Knox 2004; Hannestad et al. 2006; Kitching et al. 2008; Ichiki et al. 2009; de Bernardis et al. 2009; Jimenez et al. 2010). To this end, ongoing and planned wide-field optical surveys,

such as the DES¹, LSST², Euclid³, WFIRST⁴, HSC⁵, KIDS⁶, and Pan-STARRS⁷ surveys, will measure the shapes of hundreds of millions to billions of galaxies and thus cosmic shear signals with unprecedented statistical precision.

Given this incredible statistical power, understanding and mitigating potential systematic errors in these measurements will be very important. Systematic contamination to cosmic shear signals can arise from a variety of sources, including the process of observing and estimating galaxy shapes from pixelated images (e.g., Kaiser 2000; Bernstein & Jarvis 2002; Vale et al. 2004; Hoekstra 2004; Guzik & Bernstein 2005; Paulin-Henriksson et al. 2008; Cypriano et al. 2010; Voigt & Bridle 2010; Kacprzak et al. 2012; Refregier et al. 2012; Voigt et al. 2012; Antonik et al. 2012) or estimating photometric redshifts (e.g., Ma et al. 2006; Huterer et al.

¹ The Dark Energy Survey - <http://www.darkenergysurvey.org>

² Large Synoptic Survey Telescope - <http://www.lsst.org>

³ <http://sci.esa.int/euclid>

⁴ Wide-Field Infrared Survey Telescope - <http://wfirst.gsfc.nasa.gov>

⁵ Hyper Suprime-Cam - <http://www.naoj.org/Projects/HSC>

⁶ The Kilo Degree Survey - <http://kids.strw.leidenuniv.nl>

⁷ The Panoramic Survey Telescope & Rapid Response System - <http://pan-starrs.ifa.hawaii.edu>

* E-mail: beckermr@uchicago.edu

2006; Bridle & King 2007; Sun et al. 2009; Hearin et al. 2010; Bernstein & Huterer 2010; Cunha et al. 2012). There are also astrophysical sources of systematic errors, like intrinsic alignments (e.g., Heavens et al. 2000; Croft & Metzler 2000; Catelan et al. 2001; Crittenden et al. 2001, 2002; Jing 2002; Lee & Pen 2002; Hirata & Seljak 2004; Heymans et al. 2006b; Hui & Zhang 2008; Semboloni et al. 2008), source galaxy clustering (Schneider et al. 2002b), or the effects of baryons and galaxy formation on the matter power spectrum (e.g., White 2004; Zhan & Knox 2004; Huterer & Takada 2005; Jing et al. 2006; Rudd et al. 2008; Guillet et al. 2010; van Daalen et al. 2011; Casarini et al. 2011, 2012; Hearin et al. 2012). These systematic errors, if left uncontrolled, can bias and/or degrade constraints on the properties of Dark Energy or modifications to GR from future surveys (e.g., Hirata & Seljak 2003, 2004; Guzik & Bernstein 2005; Huterer & Takada 2005; Huterer et al. 2006; Mandelbaum et al. 2006a; Ma et al. 2006; Bridle & King 2007; Hirata et al. 2007; Hearin & Zentner 2009; Sun et al. 2009; Semboloni et al. 2009; Bernstein & Huterer 2010; Hearin et al. 2010; Kirk et al. 2012; Laszlo et al. 2012; Cunha et al. 2012; Hearin et al. 2012).

Besides direct image and structure formation simulations to study cosmic shear data analysis, systematics, and theoretical modeling in detail (e.g., STEP1 (Heymans et al. 2006a); STEP2 (Massey et al. 2007); GREAT08 (Bridle et al. 2010); GREAT10 (Kitching et al. 2012); Jain et al. 2000; Vale & White 2003; Lee & Pen 2008; Hilbert et al. 2009; Sato et al. 2009; Teyssier et al. 2009; Hahn et al. 2010; Kiessling et al. 2011; Harnois-Deraps et al. 2012), it is important to distinguish between observational signals which can arise from GR and those which cannot (Kaiser 1992). At first order in the gravitational potential, GR will only produce cosmic shear patterns known as E-modes (see, e.g., Dodelson 2003 for a pedagogical introduction). The complementary patterns, known as B-modes, are not produced by GR at first order, though they can be produced in small amounts at higher order (e.g., Jain et al. 2000; Cooray & Hu 2002; Vale & White 2003; Hilbert et al. 2009; Bernardeau et al. 2010; Krause & Hirata 2010). Many of the sources of systematic contamination, though not all, can produce B-modes in addition to E-modes (e.g., Crittenden et al. 2001, 2002; Schneider et al. 2002b; Vale et al. 2004; Hirata & Seljak 2004; Jarvis & Jain 2004; Guzik & Bernstein 2005; Antonik et al. 2012). Therefore assessing B-mode contamination in cosmic shear signals can test for systematic errors throughout the various steps of cosmic shear data analysis, from observing the galaxies with a telescope and imaging camera, all the way through to the theoretical modeling and constraints on cosmological parameters.

Methods for separating E- and B-modes in cosmic shear data have been studied extensively by previous authors. Broadly, these methods either operate directly on the shear field (Schneider et al. 1998; Seljak 1998; Hu & White 2001; Heavens 2003; Leonard et al. 2012) or on the shear two-point correlation functions (Crittenden et al. 2002; Schneider et al. 2002b; Schneider & Kilbinger 2007; Schneider et al. 2010; Fu & Kilbinger 2010). E/B-mode separation in the context of higher-order correlation functions has been studied as well (Jarvis et al. 2004; Schneider et al. 2005; Shi et al. 2011; Krause et al. 2012). Additionally, techniques originally designed for the analysis of Cosmic Microwave Background polarization signals (e.g., Wandelt et al. 2001; Smith 2006) can also be applied to cosmic shear (Hikage et al. 2011). Importantly, the details of the implementation of these methods can effect their performance significantly (e.g., Smith 2006; Kilbinger et al. 2006). For the

shear two-point correlation functions, $\xi_{\pm}(\theta)$ defined below, Schneider & Kilbinger (2007) have shown that a broad class of E/B-mode statistics, can be written in the following form

$$E_c = \frac{1}{2} \int_L^H d\theta \theta [T_+(\theta)\xi_+(\theta) + T_-(\theta)\xi_-(\theta)]$$

$$B_c = \frac{1}{2} \int_L^H d\theta \theta [T_+(\theta)\xi_+(\theta) - T_-(\theta)\xi_-(\theta)].$$

By choosing the range of integration $[L, H]$ and the forms of $T_{\pm}(\theta)$ properly, one can show that E_c will contain only E-mode information and B_c will contain only B-mode information either over an infinite interval or finite interval with $L > 0$ (Schneider & Kilbinger 2007). Note that these statistics assume one has continuous shear correlation function data.

Practical implementations of the E_c and B_c statistics in cosmic shear data analysis are constrained in several ways. The shear correlation functions are usually estimated in bins of angle, say N bins, with some effective binning weight $W_i(\theta)$. In particular, the expectation value of the estimated shear correlation function data point for the i th bin is (e.g., Schmidt et al. 2009)

$$\langle \widehat{\xi}_{\pm i} \rangle = \int_{L_i}^{H_i} d\theta W_i(\theta) \xi_{\pm}(\theta). \quad (1)$$

The form of these binning functions and this result is discussed below and in Appendix A. Thus the statistics E_c and B_c in this case must be estimated from the binned shear correlation function data, $\widehat{\xi}_{\pm i}$. Also, in order for the statistics E_c and B_c to remain pure two-point statistics, any procedure for estimating them from cosmic shear data can only consider linear combinations of the binned shear correlation function data,

$$X_{\pm} = \frac{1}{2} \sum_i \left[F_{+i} \widehat{\xi}_{+i} \pm F_{-i} \widehat{\xi}_{-i} \right], \quad (2)$$

where the $F_{\pm i}$ are constants which describe the statistics (see e.g., Kilbinger & Munshi 2006).

In this work, I study the use of these linear combinations for E/B-mode separation and thus the effects of these constraints on cosmic shear data analysis. In particular, after covering the basics of cosmic shear in Section 2, I demonstrate in Section 3.1 that *even if the statistics E_c and B_c contain pure E- and B-mode information, the statistics X_{\pm} generally exhibit E/B-mode mixing due to the binning*. In Section 3.2, I show how to define the statistics X_{\pm} through the choice of the $F_{\pm i}$, so that they suppress the E/B-mode mixing below detectable levels for any current or upcoming cosmic shear survey. In this section I also give practical recipes for computing the $F_{\pm i}$. Other potential and ultimately equivalent optimal estimator definitions are discussed in Section 3.3. I then show how to use these optimal estimators to divide the vector space of correlation function data points up into approximately ambiguous, E- and B-mode subspaces in Section 3.4. I compute the Gaussian covariances of these statistics in Section 3.5. In Sections 4.1 and 4.2, I provide two examples of these statistics to illustrate how to build and use them in practice. I provide an example of how to decompose the shear correlation functions into ambiguous, E- and B-modes and also discuss the Fisher information content of these subspaces in Section 4.3. I find that the ambiguous mode subspace has a non-trivial amount of information about typical cosmological parameters. Finally, I conclude and discuss how these statistics are applicable to blinded or closed-box cosmic shear data analyses in Section 5.

2 COSMOLOGICAL WEAK LENSING

The basic equations describing weak lensing by cosmological density fields are covered in detail in other works (see e.g., Bartelmann & Schneider 2001; Dodelson 2003; Hoekstra & Jain 2008; Bartelmann 2010). The discussion presented here is merely a summary of the relevant results needed for this work. Given the 3D density matter power spectrum $P(k, a)$ as a function of wave number k and scale factor a , the 2D convergence power spectrum as a function of 2D wave number ℓ is defined in the Limber approximation as (cf. Hoekstra & Jain 2008)

$$C_{ij}^k(\ell) = \int_0^\infty d\chi \frac{W_i(\chi)W_j(\chi)}{\chi^2} P(\ell/\chi(z), a)$$

$$W_{i,j}(\chi) = \frac{3}{2}\Omega_m \left(\frac{H_0}{c}\right)^2 \frac{\chi}{a(\chi)} \int_\chi^\infty d\chi_s \frac{n_{i,j}(\chi_s)}{\bar{n}_{i,j}} \frac{\chi_s - \chi}{\chi_s}$$

where z is the redshift, $\chi(z)$ is the comoving distance, and $n_i(\chi)$ is the redshift distribution of the lensing sources for source set i normalized to the total source density, $\bar{n}_{i,j} = \int d\chi_s n_{i,j}(\chi_s)$. These expressions assume straight-line photon paths from the sources to the observer, commonly called the Born approximation, and a spatially flat universe. I use the non-linear power spectrum fitting formula of Smith et al. (2003) to compute C_{ij}^k and the fitting formula of Eisenstein & Hu (1998) to evaluate the linear power spectrum. Additionally, in this work all lensing sources are at a single redshift, $z_s = 1.0$, such that $\bar{n}(\chi_s) = \delta(\chi_s - \chi(z_s))$, where $\delta(\chi)$ is the Dirac delta function.

In cosmological weak lensing, one observes the shear field (neglecting reduced shear effects, see e.g., Schneider & Seitz 1995; Mandelbaum et al. 2006b) along with an assumed to be random contribution from galaxy shapes and orientations. This last effect is commonly called shape noise and is characterized by the shape noise per component, σ_e . The breaking of the assumption of random galaxy orientations is generically referred to as intrinsic alignments and is a primary source of systematic error in cosmic shear measurements (see the references given above). Given the complex shear field, $\gamma = \gamma_1 + i\gamma_2$, one can define the ξ_\pm correlation functions as (cf. Schneider et al. 2002b)

$$\xi_+ = \langle \gamma_t \gamma_t \rangle + \langle \gamma_\times \gamma_\times \rangle$$

$$\xi_- = \langle \gamma_t \gamma_t \rangle - \langle \gamma_\times \gamma_\times \rangle$$

where $\gamma_t = -\text{Re}(\gamma e^{-2i\phi})$, $\gamma_\times = -\text{Im}(\gamma e^{-2i\phi})$, and ϕ is the polar angle of the vector connecting the two points. In Appendix A, I present the standard expressions for galaxy pair-wise shear correlation function estimators and their expectation values (see, e.g., Schneider et al. 2002a; Schmidt et al. 2009).

In Fourier-space, the shear field is typically separated into a component with no net handedness, the E-mode part, and a handed component, the B-mode part. In terms of the power spectra of the E- and B-mode parts, these correlation functions are (cf. Schneider & Kilbinger 2007)

$$\xi_+(\theta) = \int_0^\infty \frac{d\ell \ell}{2\pi} J_0(\ell\theta) [P_E(\ell) + P_B(\ell)] \quad (3)$$

$$\xi_-(\theta) = \int_0^\infty \frac{d\ell \ell}{2\pi} J_4(\ell\theta) [P_E(\ell) - P_B(\ell)] \quad (4)$$

where the $J_n(\ell\theta)$ are cylindrical Bessel functions. In the Born approximation, the B-mode power is identically zero, $P_B(\ell) \equiv 0$, and the E-mode power is equal to the convergence power spectrum, $P_E(\ell) = C_{ij}^k$. Corrections to the Born approximation are very small (e.g., Jain et al. 2000; Cooray & Hu 2002; Vale & White

2003; Hilbert et al. 2009; Bernardeau et al. 2010; Krause & Hirata 2010). The shape noise contribution to the power spectra, σ_e^2/\bar{n} , has been purposefully left out of these expressions because pair-wise estimators of the shear correlation functions (see Appendix A) do not exhibit noise biases (Schneider et al. 2002a).

Finally, the covariance of the shear-shear correlation functions can be computed under the assumption that the shear fields are Gaussian with the following expressions from Joachimi et al. (2008)

$$\langle \xi_{+/-}(\theta_1) \xi_{+/-}(\theta_2) \rangle =$$

$$\frac{1}{\pi\Omega_s} \int_0^\infty d\ell \ell J_{0/4}(\ell\theta_1) J_{0/4}(\ell\theta_2) \times \left\{ P_E^2(\ell) + P_B^2(\ell) + \frac{2\sigma_e^2}{\bar{n}} [P_E(\ell) + P_B(\ell)] \right\} + \delta_{\theta_1\theta_2} \frac{4\sigma_e^4}{\bar{n}^2 2\pi\theta_1 \Delta\theta_1 \Omega_s}$$

$$\langle \xi_+(\theta_1) \xi_-(\theta_2) \rangle =$$

$$\frac{1}{\pi\Omega_s} \int_0^\infty d\ell \ell J_0(\ell\theta_1) J_4(\ell\theta_2) \times \left\{ P_E^2(\ell) + P_B^2(\ell) + \frac{2\sigma_e^2}{\bar{n}} [P_E(\ell) + P_B(\ell)] \right\} \quad (5)$$

where $\Delta\theta_1$ is the bin width and Ω_s is the survey area. Note that the shape noise contributes to cross terms in braces in addition to the diagonal terms given by the Kronecker delta function. The covariance between ξ_+ and ξ_- is given by second of the above expressions.

The expressions for the correlation function covariance matrix will be useful below for computing the Fisher information content of the shear correlation functions under the assumption the errors are Gaussian. The Fisher information matrix is (e.g., Tegmark et al. 1997)

$$F_{ij} = \frac{1}{2} \text{Tr} [A_i A_j + C^{-1} M_{ij}] \quad (6)$$

where C is the covariance matrix of the observations, $A_i = C^{-1} C_{,i}$, and $M_{ij} = \vec{\mu}_{,i} \vec{\mu}_{,j}^T + \vec{\mu}_{,j} \vec{\mu}_{,i}^T$. Here $\vec{\mu}$ is the vector of mean values of the data and the notation $,i$ indicates a partial derivative with respect to parameter θ_i . Below I neglect the information in the covariance matrix so that the Fisher information is computed only using the last term in the equation above. There are several conventions in the literature for comparing the Fisher information content of various analyses. I roughly follow Schneider et al. (2010) and simply compare various analyses by computing $f \equiv \sqrt{|F|}$ for a fiducial set of parameters for each analysis. I use σ_8 , the normalization of the linear matter power spectrum today filtered in $8 h^{-1} \text{Mpc}$ spheres, and Ω_m , the mean matter density today in units of the critical density, as the fiducial set of parameters for comparison. These Fisher information estimates are not meant to be realistic survey projections, but to give a sense of how much of the total Fisher information is retained by the E/B-mode statistics presented in this paper.

Throughout this work I assume a flat Λ CDM universe with $\Omega_m = 0.25$, $H_0 = h^{-1} 100 \text{ kms}^{-1} \text{Mpc}^{-1}$, $h = 0.7$, $\sigma_8 = 0.8$, $n_s = 1.0$, and $\Omega_b = 0.044$. Also, I consider two different prototypical weak lensing surveys with different areas, Ω_s , and lensing source number densities, \bar{n} . The first survey has $(\Omega_s, \bar{n}) = (5000 \text{ deg}^2, 10 \text{ gals/arcmin}^2)$, typical of the DES and the second has $(\Omega_s, \bar{n}) = (20,000 \text{ deg}^2, 40 \text{ gals/arcmin}^2)$, typical of the LSST survey. I set the lensing shape noise per component to $\sigma_e = 0.3$ for both the DES- and LSST-like surveys.

3 E/B-MODE ESTIMATION WITH BINNED DATA

In this section I study the problem of E/B-mode estimation with binned cosmic shear data in detail. I show that generally estimators which are linear combinations of the binned cosmic shear data points mix E- and B-mode signals. I then demonstrate how to define optimal estimators which minimize this E/B-mode mixing and give practical recipes for constructing and using these estimators. Next I discuss other potential optimal estimator definitions, demonstrating that they are approximately equivalent to the definition used throughout this work. Then I discuss how to decompose the vector space composed of the binned shear correlation functions into approximately ambiguous, E- and B-mode subspaces. Finally, I compute the variance and covariance of these estimators under the assumption the shear power spectra are Gaussian.

3.1 Binned Data & E/B-mode Mixing

As stated above, shear correlation functions are typically measured in a bins of angle so that $\theta \in [L_i, H_i]$ for the i th bin. Additionally, for the standard shear two-point function estimator, the shear correlation function measurements are weighted by the bin weighting function $W_i(\theta)$, as in Equation (1). Generally these bin weighting functions are normalized to unity so that $\int_{L_i}^{H_i} d\theta W_i(\theta) = 1$. Throughout this work I assume the bin weighting functions are normalized properly. As detailed in Appendix A, for pair-wise estimators of the shear correlation functions this bin weighting function is in general quite complicated because of the survey window function and source galaxy clustering. Note however that for unclustered sources and neglecting the survey window function, $W_i(\theta) = 2\theta/(H_i^2 - L_i^2)$, so that the dominant effect is a purely geometric weighting. This effect arises from the increase in the number of galaxy pairs due to the increase in the area in the outer part of the bin relative to the inner part. I show in Appendix A that by using small enough bins, the effects of the source clustering can be made negligible. Assessing the form and magnitude of the weightings from the survey window function is beyond the scope of this work. Thus when needed, I only use the geometric weightings given above.

Given the bin window functions, I now consider statistics which are general linear combinations of the shear correlation function data points described by Equation (2). The form of these statistics has been chosen for easy comparison with work for E/B-mode statistics for unbinned shear correlation function data presented by Schneider & Kilbinger (2007). It is important to realize however that I have included a bin size dependent weight through the normalization of the $W_i(\theta)$ in the definition of the statistics unlike Schneider & Kilbinger (2007). The correspondence between the F_{\pm} coefficients, which define the statistics X_{\pm} , and the $\{E_c, B_c\}$ statistics presented in Schneider & Kilbinger (2007) is $T_{\pm}(\theta) = W_i(\theta)F_{\pm i}/\theta$ for each bin i .

I will now show that *the statistics X_{\pm} always mix E- and B-mode information*, barring a very special choice of the bin window functions $W_i(\theta)$. This derivation follows closely a derivation presented in Schneider & Kilbinger (2007), but accounts for the binning explicitly. In order to proceed, I substitute the definitions of the shear correlation functions in terms of the E- and B-mode power spectra from Equations (3) and (4) into the definition of X_{\pm} to get the following expression for the expectation value of the statistics

$$\langle X_{\pm} \rangle = \int_0^{\infty} \frac{d\ell \ell}{2\pi} P_E(\ell) W_{\pm}(\ell) + P_B(\ell) W_{\mp}(\ell) \quad (7)$$

$$W_{\pm}(\ell) = \frac{1}{2} \sum_i \left(F_{+i} \int_{L_i}^{H_i} d\theta W_i(\theta) J_0(\ell\theta) \pm F_{-i} \int_{L_i}^{H_i} d\theta W_i(\theta) J_4(\ell\theta) \right) \quad (8)$$

These equations with $P_B(\ell) \equiv 0$ were presented by Kilbinger & Munshi (2006). The statistic X_+ will have no B-mode contribution if $W_-(\ell) = 0$ for all ℓ and thus would be an E-mode statistic. Similarly, X_- would be a B-mode statistic. Setting $W_-(\ell) = 0$, I can integrate over ℓ against $\ell J_4(\ell\phi)$ to get

$$\begin{aligned} \sum_i F_{-i} \int_{L_i}^{H_i} d\theta W_i(\theta) \int_0^{\infty} d\ell \ell J_4(\ell\theta) J_4(\ell\phi) \\ = \sum_i F_{+i} \int_{L_i}^{H_i} d\theta W_i(\theta) \int_0^{\infty} d\ell \ell J_0(\ell\theta) J_4(\ell\phi). \end{aligned}$$

This equation must hold for arbitrary ϕ . Now let $\phi \in [L_k, H_k]$. Using the closure relationship for the Bessel functions

$$\int_0^{\infty} d\ell \ell J_4(\ell\theta) J_4(\ell\phi) = \frac{1}{\phi} \delta(\theta - \phi) \quad (9)$$

and the following result from Schneider et al. (2002b)

$$\begin{aligned} G(\theta, \phi) &= \int_0^{\infty} d\ell \ell J_0(\ell\theta) J_4(\ell\phi) \\ &= \left(\frac{4}{\phi^2} - \frac{12\theta^2}{\phi^4} \right) H(\phi - \theta) + \frac{1}{\phi} \delta(\phi - \theta), \end{aligned}$$

I get the following expression for F_{-k} in terms of the F_{+i}

$$\begin{aligned} F_{-k} &= F_{+k} + \frac{\phi}{W_k(\phi)} \\ &\times \sum_{i \leq k} F_{+i} \int_{L_i}^{\min(H_i, \phi)} d\theta W_i(\theta) \left(\frac{4}{\phi^2} - \frac{12\theta^2}{\phi^4} \right). \end{aligned} \quad (10)$$

Here $H(\phi - \theta)$ is the Heaviside step function and $\delta(\phi - \theta)$ is the Dirac delta function. This equation is the discrete analog of the results presented in Schneider & Kilbinger (2007). In fact, it can be obtained by setting the quantities $T_{\pm}(\phi)$ from Schneider & Kilbinger (2007) to $W_i(\phi)F_{\pm i}/\phi$ in each bin $[L_i, H_i]$.

Originally I assumed that the $F_{\pm i}$ were constants not functions of ϕ , but the equation derived above in general has dependence on ϕ . Therefore generally $W_-(\ell)$ will not be identically zero for all ℓ . The only way to ensure $W_-(\ell) \equiv 0$ is to pick the bin window functions $W_i(\phi)$ so that they exactly cancel the ϕ dependence in the equation above and then use this equation to compute the F_{-i} in terms of the F_{+i} . Apart from this caveat, statistics of the form X_{\pm} will mix E- and B-mode information in general. This mixing arises directly from the binning and is a general feature of E/B-mode separation with pixelized data as well (see e.g., Smith 2006; Lin et al. 2011).

These results have important implications for the theoretical analysis of binned cosmic shear correlation function data. For binned shear correlation functions with N bins, it would be nice to divide the space of the $2N$ data points into pure E-mode, pure B-mode, and ambiguous modes, similar to the decomposition achieved by Schneider et al. (2010) with the COSEBI statistics over the continuous function space of the shear correlation functions. However, I have shown that for general window functions $W_i(\theta)$, this decomposition is impossible because there do not exist pure E-

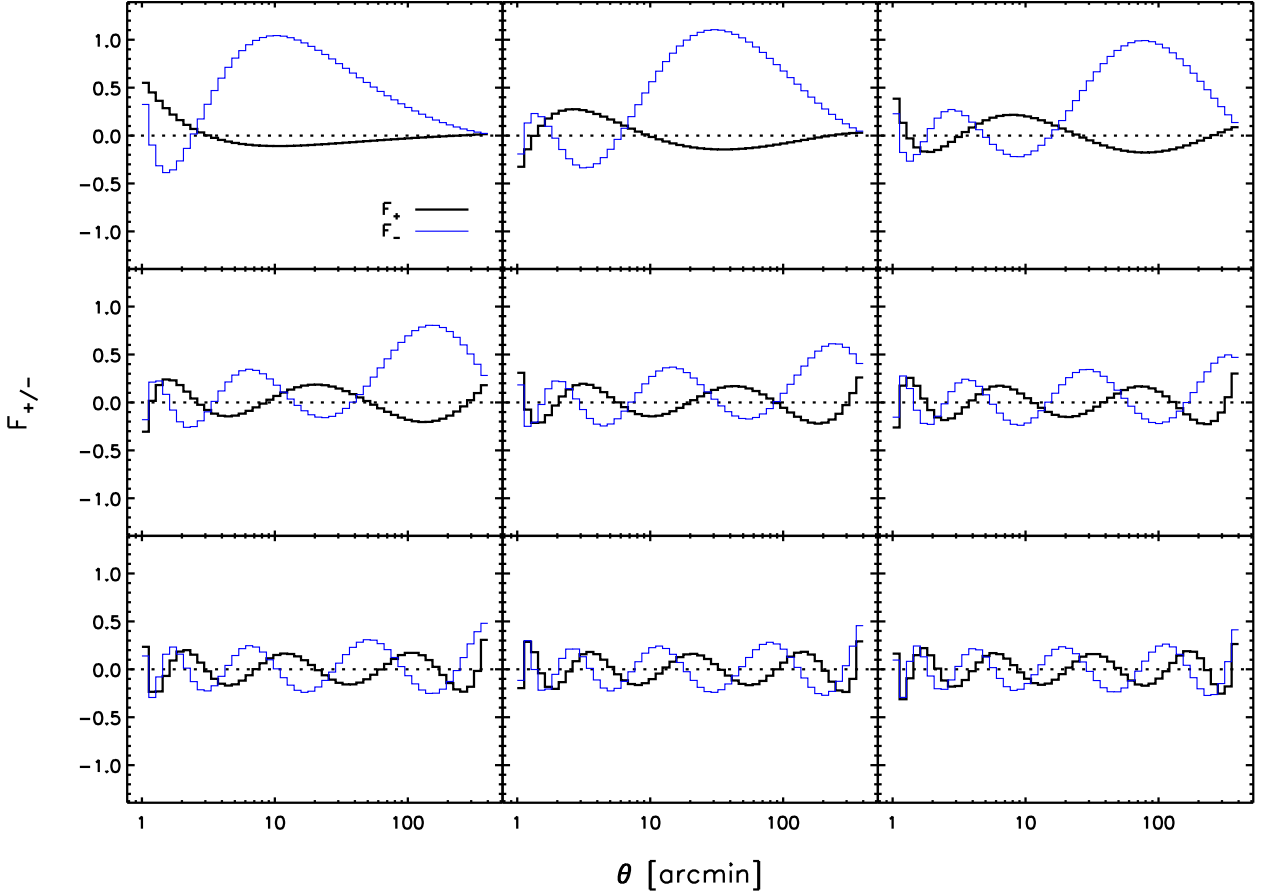


Figure 1. The first nine components of the COSEBI-like basis for 50 shear correlation function data points with $\theta \in [1, 400]$ arcmin. The thick black lines show the F_{+} filters and the thin blue lines show the F_{-} filters. Each set of F_{\pm} filters has been normalized to the same scale in each panel.

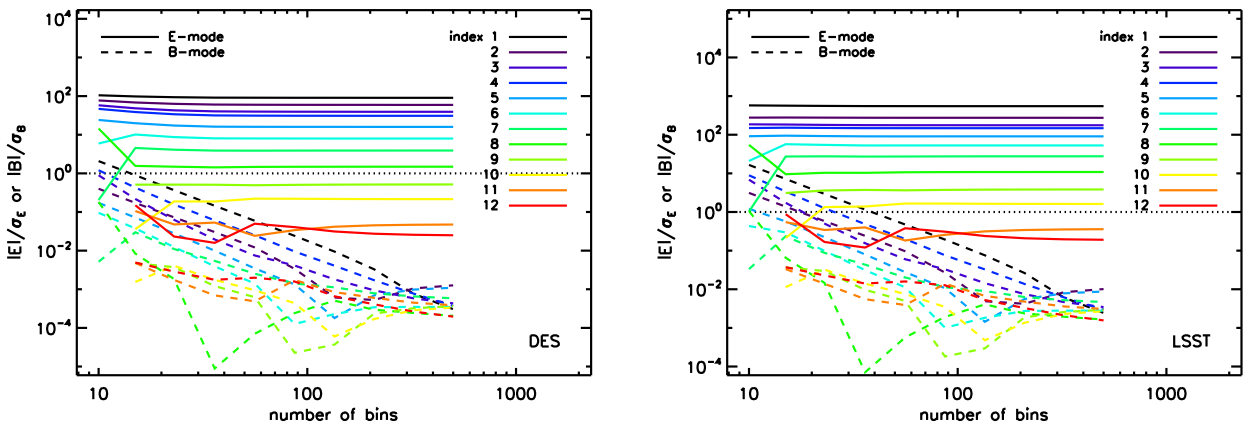


Figure 2. The signal-to-noise of the COSEBI-like E- and B-mode statistics as a function of the number of shear correlation function bins. The solid lines show from top to bottom the signal-to-noise of the first 12 E-mode statistics (estimated using only the diagonal elements of the covariance matrix). The dashed lines show the signal-to-noise in the B-mode statistics. The dotted line in each panel marks a signal-to-noise of unity. The left panel is for a DES-like survey, while the right panel is for an LSST-like survey. The intrinsic B-mode power was set to zero for this computation, so any statistically significant B-mode statistics are due purely to E/B-mode mixing. This mixing decreases as the number of shear correlation function bins increases. Additionally, the fact that only $\sim 8 - 10$ of the E-mode statistics are statistically significant illustrates the data compression properties of these statistics.

and B-mode linear combinations. In the next section, I will define approximately pure E- and B-mode linear combinations, along with approximately ambiguous modes. Thus I will show that there does in fact exist a division of the space of $2N$ data points into *approximately* ambiguous, E- and B-mode subspaces. This approximate decomposition is explored fully in Section 3.4.

These results are also quite useful for cosmic shear data analysis. Suppose one did in fact use a statistic which is a linear combination of the shear correlation function data points. Then from Equations (7) and (8) one can compute how the statistic mixes E- and B-modes due to the binning. Additionally as I will show below, as the shear correlation function bins are made smaller, the magnitude of $W_-(\ell)$ will decrease, so that the E/B-mode mixing decreases as well. If the bins are made small enough, the bias in X_- , the B-mode statistic, due to E/B-mode mixing, can be made smaller than the statistical errors. Thus these results give a quantitative criterion by which to decide the number and size of the bins used to compute the shear correlation functions. Finally, Equation (10) suggests two ways to minimize the E/B-mode mixing. The first is to reweight the data in each bin by choosing the $W_i(\phi)$ to cancel the ϕ dependence in Equation (10) and then use this equation to compute the F_{-i} . I will not consider this possibility here. The second is to pick the F_{-i} in order to minimize the E/B-mode mixing without adjusting the bin window functions. Given a fiducial choice for the F_{+i} , one can define F_{-i} in some way (roughly similar to Equation (10)) in order to minimize the mode mixing by minimizing $W_-(\ell)$. The details of this definition along with a general procedure for computing the $F_{\pm i}$ are described in the next section.

3.2 Building Binned E/B-mode Estimators

Consider now binned shear correlation function data over the range $[L, H]$ in angle with N bins. Each bin is described by the bin window functions introduced above so that the bins cover the range $[L, H]$ without any overlaps between the ranges of each bin, $[L_i, H_i]$. In order to define the F_{-k} , I minimize the square amplitude of the window function $W_-(\ell)$ with respect to the coefficients F_{-k} ,

$$0 = \frac{\partial}{\partial F_{-k}} \left[\int_0^\infty d\ell \ell |W_-(\ell)|^2 \right]. \quad (11)$$

The solution to this equation is

$$\begin{aligned} F_{-k} = F_{+k} + & \left(\int_{L_k}^{H_k} d\theta \frac{W_k^2(\theta)}{\theta} \right)^{-1} \sum_i F_{+i} \\ & \times \int_{L_i}^{H_i} \int_{L_k}^{H_k} d\theta d\phi W_i(\theta) W_k(\phi) \\ & \times \left(\frac{4}{\phi^2} - \frac{12\theta^2}{\phi^4} \right) H(\phi - \theta). \end{aligned} \quad (12)$$

This solution is equivalent to multiplying Equation (10) by $W_k(\phi)/\phi$ and then integrating over ϕ with the weight $W_k(\phi)$.

Similarly to the unbinned estimators described in Schneider & Kilbinger (2007), the binned estimators described in this work must satisfy two integral constraints in order to be non-zero only over a finite range in angle. These constraints can be understood as follows. Suppose that the F_{+i} are non-zero only in the interval $[L_s, H_s]$ contained in $[L, H]$. Now consider $\phi \geq H_s$.

Then according to Equation (12), the F_{-i} will be non-zero in the interval $[L_s, H_s]$ only if the F_{+i} satisfy the following constraints

$$0 = \sum_{\theta_i \in [L_s, H_s]} F_{+i} \int_{L_i}^{H_i} d\theta W_i(\theta) \quad (13)$$

$$0 = \sum_{\theta_i \in [L_s, H_s]} F_{+i} \int_{L_i}^{H_i} d\theta W_i(\theta) \theta^2 \quad (14)$$

where the sums run only over bins in the interval $[L_s, H_s]$. Given data in some fiducial angular interval, one can always increase the angular range considered as long as the $F_{\pm i}$ are zero outside the fiducial angular range. Thus in order for the X_{\pm} statistics to self-consistently consider only data in a finite angular range and minimize E/B-mode mixing by minimizing $W_-(\ell)$, they must satisfy the constraints given above.

As discussed in Schneider et al. (2010), these constraints serve to project out ambiguous modes in the continuous correlation functions ξ_{\pm} which cannot be uniquely classified as either E- or B-modes. These modes are $\xi_+(\theta) = a + b\theta^2$ and so these constraints simply project out the binned versions of these modes. Barring the caveat discussed above, in the discrete case no modes can be uniquely classified as pure E- or B-modes. Thus in this sense all modes are ambiguous in the discrete case, due to the binning. However, E/B-mode separation for the discrete modes along $\xi_+(\theta) = a + b\theta^2$ is not possible even in the limit of infinitely small bins, so these discrete modes are the analogues of the ambiguous continuous modes. Importantly, these ambiguous modes can still potentially carry cosmological information, it is just that one cannot uniquely determine if the modes are sourced by the E- or B-mode power spectrum. Assuming one has determined that the cosmic shear data is free of systematic contamination, it may be advantageous to keep and use the information in the ambiguous modes (see Smith 2006 for a similar point in the context of the pseudo- C_ℓ formalism and also Schneider et al. 2010). This point is illustrated below with a simple Fisher information analysis.

Given the linear relation between the $F_{\pm i}$ and the linear constraints on the F_{+i} , it is natural to treat them as vectors of length N . Thus the two integral constraints in Equations (13) and (14) mean that the F_+ vector cannot have any component along the directions

$$\begin{aligned} F_{+a} &= \left(\int_{L_1}^{H_1} d\theta W_1(\theta), \int_{L_2}^{H_2} d\theta W_2(\theta), \dots, \right. \\ & \quad \left. \int_{L_N}^{H_N} d\theta W_N(\theta) \right)_N \\ F_{+b} &= \left(\int_{L_1}^{H_1} d\theta W_1(\theta) \theta^2, \int_{L_2}^{H_2} d\theta W_2(\theta) \theta^2, \dots, \right. \\ & \quad \left. \int_{L_N}^{H_N} d\theta W_N(\theta) \theta^2 \right)_N. \end{aligned}$$

Similarly, Equation (12) defines a matrix, which I will denote as M_+ , which relates the F_+ to the F_- via $F_- = M_+ F_+$. I give explicit forms for these quantities assuming geometric bin weightings in Appendix B.

The overall process to create a set of F_+ and F_- vectors and measure the E- and B-mode signals in this scheme is quite straightforward.

(1) Choose an initial shape for the F_+ vector. Usually one has some external motivation for this choice, like for example, statistics which form a complete set of functions and exhibit efficient

data compression (Schneider et al. 2010), statistics that are compact and non-oscillatory in Fourier space (Leonard et al. 2012), or statistics which maximize the signal-to-noise in the measurement of cosmological parameters, like σ_8 or Ω_m (Fu & Kilbinger 2010).

(2) Make F_+ is orthogonal to the F_{+a} and F_{+b} vectors defined above. In practice, an efficient way to do this is to first make F_{+a} and F_{+b} orthogonal to one another by modifying F_{+b} . Then it is easy to make F_+ orthogonal to both F_{+a} and the modified F_{+b} by projecting out the components of F_+ along the modified constraint directions.

(3) Use the matrix M_+ defined in Equation (12) to compute the corresponding F_- filter via $F_- = M_+ F_+$.

(4) Compute the E- and B-mode signals by forming the vector inner product of the binned $\hat{\xi}_{\pm}$ shear correlation function data with the F_{\pm} filters. Then $E = X_+ = (I_+ + I_-)/2$ and $B = X_- = (I_+ - I_-)/2$, where $I_{\pm} = \sum_i \hat{\xi}_{\pm i} F_{\pm i}$.

Below I use both the procedure just described and also Gram-Schmidt orthogonalization to define F_+ functions. In the case of Gram-Schmidt orthogonalization, one simply uses F_{+a} and F_{+b} first in the Gram-Schmidt process, followed by the rest of the initial estimator shapes for F_+ . The result of applying the Gram-Schmidt procedure is a set of orthogonal F_+ filters contained in the $N - 2$ elements of the orthogonal basis. The first two elements of this basis span the space generated by the constraint directions F_{+a} and F_{+b} . The F_- filters are again obtained from the matrix defined in Equation (12).

3.3 Other Potential Optimal Estimator Definitions

In this section I will explore two other potential optimal estimator definitions. The first definition simply consists of swapping the roles of F_+ and F_- in the previous section. Thus in this scheme the optimal estimator is now defined by

$$0 = \frac{\partial}{\partial F_{+k}} \left[\int_0^{\infty} d\ell \ell |W_-(\ell)|^2 \right]. \quad (15)$$

The full estimators for this case are presented in Appendix C. In this case, all of the same results presented above hold and in particular there exists a matrix M_- which defines the F_+ in terms of the F_- via $F_+ = M_- F_-$. There also exist ambiguous modes, F_{-a} and F_{-b} , in analogy to the ones defined above. Finally, the procedure just given for E/B-mode separation can be carried out in exactly the same way as described above by first defining fiducial F_- filters, projecting out the F_{-a} and F_{-b} modes, computing the F_+ filters from the matrix M_- , and then computing X_{\pm} .

The second potential optimal estimator definition consists of minimizing the power in the $W_-(\ell)$ window function by varying both F_+ and F_- simultaneously. The two equations that must be solved for this kind of estimator are

$$\begin{aligned} 0 &= \frac{\partial}{\partial F_{-k}} \left[\int_0^{\infty} d\ell \ell |W_-(\ell)|^2 \right] \\ 0 &= \frac{\partial}{\partial F_{+k}} \left[\int_0^{\infty} d\ell \ell |W_-(\ell)|^2 \right]. \end{aligned}$$

Using the results for the two optimal estimators already presented, the two equations the F_{\pm} vectors must satisfy are

$$\begin{aligned} F_- &= M_+ F_+ \\ F_+ &= M_- F_- . \end{aligned}$$

Combing these two relations one gets that the optimal F_+ and F_- vectors computed in this way must satisfy

$$\begin{aligned} 0 &= (M_- M_+ - I) F_+ \\ 0 &= (M_+ M_- - I) F_- , \end{aligned}$$

where I is the identity matrix. Thus in this case the F_{\pm} vectors must be in the null space or kernels of the matrices $M_{\mp} M_{\pm} - I$.

A straight forward way to investigate the kernels of these matrices is via computing their Singular Value Decomposition (SVD) (e.g., Press et al. 1992). The SVD of a matrix M is defined as $M = U \Sigma V^T$. Here U and V are orthogonal matrices, assuming M is real, and Σ is a diagonal matrix with the singular values along the diagonal. One can show that a basis for the kernel of a square matrix can be found by using all of the columns of V which have zero singular values in Σ . Similar results hold for non-square matrices but they are of no use here. Additionally, the rank of the matrix is number of non-zero singular values so that a square matrix with all non-zero singular values has full rank and is invertible.

Using logarithmic binning and the geometric bin weighting $W_i(\theta)$, I find that the matrix $M_- M_+ - I$ has two large singular values which exceed all of the others by several orders of magnitude. The $N - 2$ other singular values are of similar magnitude to each other, but much smaller than the largest two. The difference between the two largest and the other $N - 2$ singular values increases as the number of bins is increased in a fixed angular range. Also, the columns of V along the two largest singular values are approximately along the ambiguous directions F_{+a} and F_{+b} . Analogous properties hold for the singular values of the matrix $M_+ M_- - I$ and the ambiguous directions F_{-a} and F_{-b} . Unfortunately, all of the singular values of these matrices are non-zero so that no vector except the zero vector lies in their null spaces. Note that one must be careful to account for rounding errors when considering whether or not singular values are zero. I find however that the $N - 2$ smaller singular values are well above rounding errors. Thus optimal estimators defined by varying both the F_+ and F_- coefficients simultaneously do not exist in this case.

However, this analysis does provide useful insight into the relationship between the estimators defined by varying F_- and those defined by varying the F_+ coefficients. In particular, given that the singular values along the directions orthogonal to the ambiguous directions $\{F_{+a}, F_{+b}\}$ and $\{F_{-a}, F_{-b}\}$ are very small, we have that F_+ and F_- vectors orthogonal to these directions span subspaces which are close to being kernels of the matrices $M_{\mp} M_{\pm} - I$. Thus

$$\begin{aligned} 0 &\approx (M_- M_+ - I) F_+ \\ 0 &\approx (M_+ M_- - I) F_- . \end{aligned}$$

One can verify this property empirically as well. Therefore the matrix M_+ generates F_- vectors which are approximately in the approximate null space of $M_+ M_- - I$ and vice versa. (To see this, simply multiply the two equations above by M_+ and M_- respectively and use the relationship $F_{\mp} = M_{\pm} F_{\pm}$.) Thus F_- vectors generated from F_+ vectors are very close to being orthogonal to the constraint directions $\{F_{-a}, F_{-b}\}$. The analogous property holds for F_+ vectors generated from F_- vectors and the constraint directions $\{F_{+a}, F_{+b}\}$. Additionally, due to these approximate equalities, the operation of ‘‘composing’’ the two different estimator definitions approximately returns the identity. In other words, one can first compute optimal estimators by varying the F_- and supplying fiducial guesses for the F_+ . Then the computed F_- vectors can be used to supply fiducial guesses for the set of optimal estimators de-

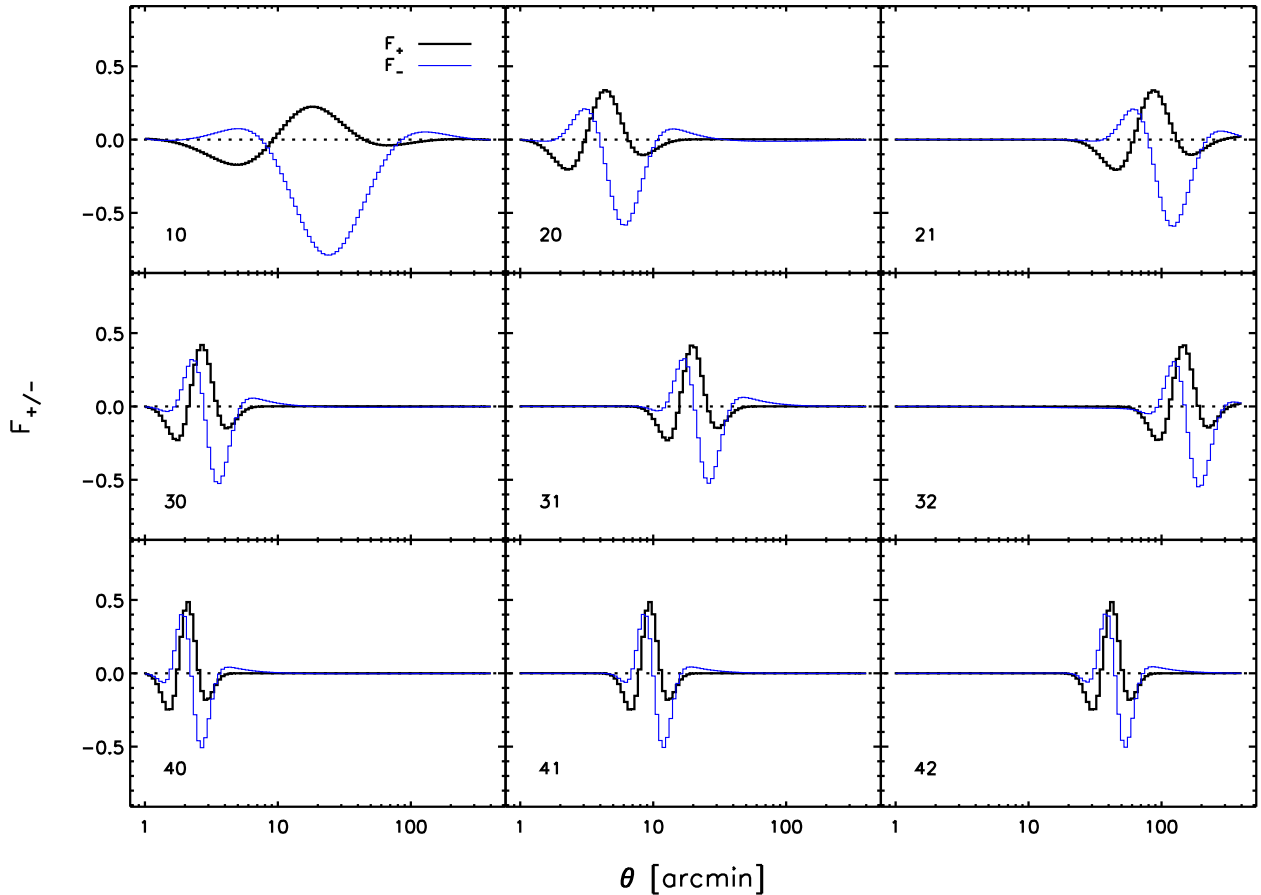


Figure 3. The first nine components of the wavelet-like estimators for 100 correlation function data points and $\theta \in [1, 400]$ arcmin. The thick black lines show the F_+ filters and the blue lines show the F_- filters. The index $\{N, i\}$ of each filter is given in the lower left corner of each panel.

fined by varying the F_+ . The new set of estimators that result from varying the F_+ will be very close to the first set of estimators defined by varying the F_- . This fact can be verified empirically. In this sense, the two optimal estimator definitions are consistent.

3.4 Approximate E-, B-, and Ambiguous Mode Decompositions for Binned Cosmic Shear Data

It is now straight forward to build the approximate decomposition of the space of $2N$ data points into E-mode, B-mode, and ambiguous modes discussed above. To do this properly, I must specify a basis for the vector space of $2N$ data points which can be divided into directions approximately along ambiguous, E- and B-modes. The subspaces spanned by each of these three sets of modes need not be mutually orthogonal, though in practice the E- and B-mode subspaces are approximately orthogonal to the ambiguous mode subspace defined below.

First, I specify the basis vectors for the ambiguous directions. These vectors are

$$\begin{aligned} & \{F_{+a}, \vec{0}\} \\ & \{F_{+b}, \vec{0}\} \\ & \{\vec{0}, F_{-a}\} \\ & \{\vec{0}, F_{-b}\} \end{aligned} \quad (16)$$

where the $\vec{0}$ are zero vectors of length N . Next I specify the E- and B-mode directions. This is done by building a set of $N - 2$ E- and B-mode estimators from a set of $N - 2$ F_+ vectors. Additionally these $N - 2$ F_+ vectors together with F_{+a} and F_{+b} should form a basis for the ξ_+ subspace of the total vector space composed of both ξ_+ and ξ_- . The construction of the optimal estimators enforces that the $N - 2$ F_+ vectors are exactly orthogonal to the F_{+a} and F_{+b} vectors. Additionally, as shown above, the resulting F_- vectors will be approximately orthogonal to the F_{-a} and F_{-b} vectors. So using the $N - 2$ F_+ vectors along with their F_- counterparts, one can define the final $2N - 4$ potential basis vectors of this space as

$$\begin{aligned} & \{F_+, +F_-\}/2 \\ & \{F_+, -F_-\}/2, \end{aligned} \quad (17)$$

where this construction is repeated for each of the $N - 2$ F_+ vectors. The first of these vectors is simply the direction of X_+ and the second is in the direction of X_- so that they are approximate E- and B-mode directions. Finally, one must verify that this set of vectors combined with the ambiguous mode directions is in fact a basis for the vectors space of dimension $2N$ by, for example, determining the rank of the matrix composed of these vectors as rows. Note that this construction would work just as well by first building a basis with the F_- vectors and the $\{F_{-a}, F_{-b}\}$ vectors, and then computing the F_+ vectors. Below, I will investigate this con-

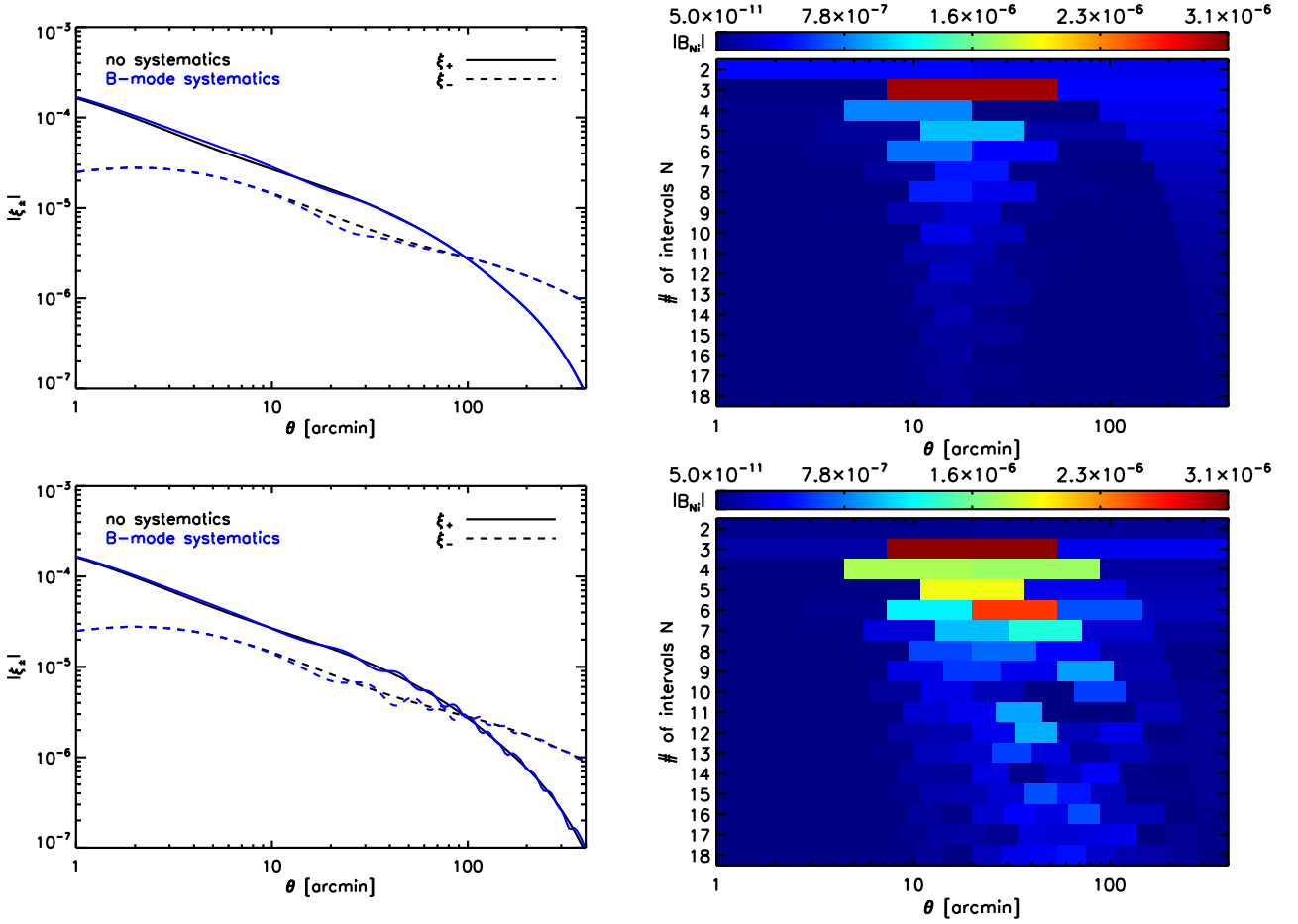


Figure 4. Example B-mode detection in noise-free data with 200 correlation function points from 1 to 400 arcmin. Each row on the left shows the underlying true correlation functions in black and the correlation functions with systematics in blue. On the right each row shows the absolute value of the wavelet-like scale-location B-mode statistics defined in Section 4.2. The vertical axis label denotes how many sections the interval [1, 400] was divided into in log-space with the intervals increasing in size from bottom to top. The interval width is reflected in the size of each colored region. The color of each region encodes the amplitude of the B-mode level. The top row has a smooth systematic signal while the bottom row has much more smaller scale variations. These finer scale variations result in B-mode detections for the smaller scale statistics for the bottom row, while no such detections are found for the top row.

struction for the COSEBI-like (Schneider et al. 2010) basis vectors defined in Section 4.1.

Finally, it is important to note that the exact properties of the matrices M_{\pm} influence the properties of the basis constructed above nontrivially. Specifically, if one uses the equal area binning (i.e. $H_i^2 - L_i^2$ is the same for all bins i), then one can show using the expressions for these matrices given in Appendices B and C for geometric binning functions that $M_- = M_+^T$. Thus for vectors along the F_{\pm} directions, the matrices M_{\pm} in this case are approximately orthogonal. A quick calculation shows that if these matrices were exactly orthogonal and one started out with an orthonormal basis for the ξ_+ subspace, then then the F_- vectors would also be orthonormal. In this case the E- and B-mode subspaces would then be exactly mutually orthogonal. In practice this exact orthogonality is not realized, but the E- and B-mode subspaces do retain some degree of orthogonality even for logarithmic binning for the COSEBI-like statistics described below in Section 4.1.

3.5 The Binned E/B-mode Estimator Covariances

With Equation (7) it is possible to compute the covariance of these statistics. I follow the same method outlined in Schneider et al. (2010) and get, assuming that the EB cross-power $P_{EB}(\ell)$ is zero and the power spectra are Gaussian,

$$\begin{aligned} \text{Cov}(E_n, E_m) = & \\ & \frac{1}{\pi\Omega_s} \int_0^{\infty} d\ell \ell \left[W_+^n(\ell) W_+^m(\ell) \left(P_E(\ell) + \frac{\sigma_e^2}{\bar{n}} \right)^2 \right. \\ & \left. + W_-^n(\ell) W_-^m(\ell) \left(P_B(\ell) + \frac{\sigma_e^2}{\bar{n}} \right)^2 \right] \end{aligned} \quad (18)$$

$$\begin{aligned} \text{Cov}(B_n, B_m) = & \\ & \frac{1}{\pi\Omega_s} \int_0^{\infty} d\ell \ell \left[W_+^n(\ell) W_+^m(\ell) \left(P_B(\ell) + \frac{\sigma_e^2}{\bar{n}} \right)^2 \right. \\ & \left. + W_-^n(\ell) W_-^m(\ell) \left(P_E(\ell) + \frac{\sigma_e^2}{\bar{n}} \right)^2 \right] \end{aligned} \quad (19)$$

$$\begin{aligned} \text{Cov}(E_n, B_m) = & \\ & \frac{1}{\pi\Omega_s} \int_0^\infty d\ell \ell \left[W_+^n(\ell) W_-^m(\ell) \left(P_E(\ell) + \frac{\sigma_e^2}{\bar{n}} \right)^2 \right. \\ & \left. + W_-^n(\ell) W_+^m(\ell) \left(P_B(\ell) + \frac{\sigma_e^2}{\bar{n}} \right)^2 \right]. \quad (20) \end{aligned}$$

These expressions reduce to those in Schneider et al. (2010) when $W_-(\ell) \equiv 0$. Also note that the squared amplitude of the $W_-(\ell)$ window function controls the amount of excess variance in the E- and B-mode statistics due to E/B-mode mixing. The procedure for defining F_- introduced above serves to minimize this excess variance. Similarly, by minimizing $W_-(\ell)$, the covariance between the E- and B-mode statistics is minimized.

4 EXAMPLES AND TESTS OF THE ESTIMATORS

In this section, I will illustrate the ideas discussed above by constructing and evaluating the performance of two different E/B-mode statistics. I first present COSEBI-like (Schneider, Eifler, & Krause 2010, hereafter SEK10) statistics in Section 4.1. These statistics have $\sim 10\times$ data compression ratios for upcoming surveys which can greatly simplify data analysis. Using these estimators I will also evaluate the level of E/B-mode mixing as function of the number of shear correlation function bins. Then I present wavelet-like B-mode statistics which allow one to determine the scale and location of B-mode contamination in shear correlation function data in Section 4.2. Finally in Section 4.3, I explore the properties of the approximate ambiguous, E- and B-mode decomposition discussed above and the Fisher information content of these subspaces using the COSEB-like statistics.

4.1 Binned COSEBI-like Estimators

As demonstrated in SEK10, filter functions which are polynomials in $\ln \theta$ have very optimal data compression ratios. Additionally, SEK10 built a set of filter functions which are orthonormal over a finite interval (using a slightly different definition of orthonormality than the vector inner product used above). In order to generate a similar set of filters for correlation functions measured with N bins, I take as an initial shape for the F_+ filters, $P_\ell(t)/\exp[(\ln \theta - \ln L)/2]$, where $P_\ell(t)$ is the Legendre polynomial of order ℓ and t is simply the logarithm of the angle θ remapped to the appropriate interval, $t \equiv 2(\ln \theta - (\ln H + \ln L)/2)/(\ln H - \ln L)$.⁸ I increase ℓ for each vector in the basis starting at $\ell = 2$ and I use the logarithmic mean of each bin interval to evaluate the polynomial. The first two vectors in the basis are the constraint directions F_{+a} and F_{+b} so that the third vector is started with $\ell = 2$. As the number of roots in the Legendre polynomials increases, they become harder to represent properly in the discrete binned space. Thus when the index of the Legendre polynomial ℓ is greater than $2N/3$, where N is the number of bins in the interval, I switch to generating the fiducial basis by producing F_+ vectors at order ℓ divided into $\ell + 1$

⁸ Note that one can discretize the SEK10 statistics directly using the correspondence between the T_\pm and F_\pm filter functions, $F_{\pm i} \sim T_\pm(\theta_i)\theta_i/W_i(\theta_i)$ where θ_i is a representative point in bin i . However, I have found that this procedure produces statistics which do not exhibit the data compression properties of the SEK10 statistics.

sections alternating between -1 and $+1$. This construction generates as many roots in the interval as the Legendre polynomial of order ℓ would have, but these roots are now resolved properly. Note that the maximum value of ℓ is $N - 1$, so that one gets exactly $N - 1$ roots when N intervals alternate between -1 and 1 . Then the Gram-Schmidt procedure is applied to the constraint vectors and the $N - 2$ fiducial F_+ vectors as described above in order to produce the final F_+ filters. The factor of $\exp[(t - \ln L)/2]$ has been inserted to roughly account for the difference between the vector inner product definition and that in SEK10. In Figure 1, I show the COSEBI-like vector basis for F_{+n} and F_{-n} for 50 shear correlation function data points between 1 and 400 arcmin.

In Figure 2, I show the level of E/B-mode mixing for these statistics as a function of the number of shear correlation function bins. I have plotted the ratio of the first 12 E- and B-mode statistics to their errors for both DES- and LSST-like surveys. Note that in general these statistics are correlated, but to make this plot I only use the diagonal contributions to the error covariance matrix. The statistics in this plot were computed with $P_B(\ell) \equiv 0$, so any nonzero B-mode statistic amplitude is completely due to E/B-mode mixing. Additionally, the E/B-mode mixing in the estimators is negligible if the nonzero amplitude of the B-mode statistic is well below the error bar on the statistic. This condition ensures that any statistically significant systematic effect is detectable and is not confused with E-modes due to E/B-mode mixing.

In general, the level of E/B-mode mixing decreases as the number of bins used for the shear correlation function increases. Additionally, it is clear that for a DES-like survey fewer shear correlation function bins can be used than for an LSST-like survey. If one uses a threshold of the B-mode statistic being no more than 10% of the 1-sigma error bar, then a DES-like survey will need of order ~ 50 bins whereas an LSST-like survey will need ~ 100 bins. This figure also demonstrates the data compression properties of these statistics. In the case of a DES-like survey of order 50 shear correlation function data points can be compressed into only ~ 8 E-mode statistics which are measurably non-zero. An LSST-like survey has increased statistical power, compressing of order 100 data points into only ~ 10 statistically significant E-mode statistics. Due to correlations between these remaining E-mode statistics, further data compression may be possible, but I will not explore this issue further in this work.

4.2 Wavelet-like B-mode Size-location Estimators

In this section, I give an example of the use of spatially-local basis functions to build sets of B-mode estimators which can pinpoint the size and location of B-mode systematics in shear correlation function data. Consider the following function, known as the Ricker wavelet (Ricker 1953),

$$\psi(t, \sigma) = \frac{2}{\sqrt{3}\sigma\pi^{1/4}} \left(1 - \frac{t^2}{\sigma^2} \right) \exp \left[-\frac{t^2}{2\sigma^2} \right]. \quad (21)$$

I take as a set of starting functions the following functions, indexed by $\{i, N\}$,

$$\begin{aligned} \phi_{iN}(t) = & \psi(t - i\Delta_N - \Delta_N/2 - \ln L, \Delta_N/8) \\ & \times \exp \left[-\frac{t - \ln L}{2} \right] \quad (22) \end{aligned}$$

where $\Delta_N = (\ln H - \ln L)/N$ and $i \in \{0, 1, \dots, N - 1\}$. This definition shifts and scales the location and size of the base wavelet so that an integer number N of them fit in the interval $[\ln L, \ln H]$

and they have most of their support in each width Δ_N subinterval of the base interval $\Delta_1 = \ln H - \ln L$. Given this starting set of smooth functions, they are turned into E- and B-mode estimators by discretizing the functions over the interval $[\ln L, \ln H]$ and then projecting out the F_{+a} and F_{+b} modes as described above. The filters which result from this process will be denoted as F_{+Ni} and F_{-Ni} . Figure 3 shows an example set of these filters for 100 correlation function data points between 1 and 400 arcmin.

In order to gain intuition into how these B-mode estimators work, I show a simple, but somewhat contrived example (however see e.g., Fu et al. 2008; Eifler et al. 2010) of two different kinds of B-mode systematics in Figure 4. The top row displays a smooth B-mode systematic in the ξ_- correlation function, while the bottom row shows a B-mode systematic with much more fine scale variations. These B-mode systematics were generated by setting $P_B(\ell)$ to be non-zero using simple Gaussian kernels, the form of which is uninteresting, and then computing the shear correlation functions using Equations (3) and (4). The contour plots show for each value of N on the vertical axis, the amplitude of the B-mode statistics for each Δ_N sized interval across the horizontal axis. In this type of analysis, a B-mode signal with more fine scale variation has a different signature than the smoother B-mode signal, with more B-mode signal detected in higher N and thus smaller sized filters. For data with shape noise, a similar contour plot can be made, except that the deviation from zero measured in units of the standard deviation should be used to produce the color scaling. The overall level of B-mode contamination can then be assessed via a χ^2 statistic computed over all of the different estimators indexed by $\{N, i\}$, accounting for the correlations between the different estimators.

Here I have chosen to layout the $F_{\pm Ni}$ filters in a simple geometric pattern. However, when a B-mode signal crosses between two filters, the significance drops. Thus it might be more advantageous to consider sets of filters which shift and scale in size more continuously. I leave this generalization to future work. Note however that the filters I have presented here are offset between different levels N so that in practice, no B-mode signal ever goes completely undetected. This general point can be clearly illustrated by examining the Fourier-space filters $W_+(\ell)$ introduced above for the wavelet-like $F_{\pm Ni}$ statistics. These filters for $N \in \{2, 3, 4\}$ are shown in Figure 5. The peaks and troughs for each N correspond to a single location of the filter in real space, with N peaks and troughs present for the N -indexed filters. As the filters shift in real space over the shear correlation function range, they cover different, but overlapping ranges in Fourier space. Thus by combining filters of different size and location, any B-mode signals in Fourier space will produce a nonzero amplitude in these filters.

4.3 Fisher Information Content and Full Mode Decomposition with COSEBI-like Statistics

In this section I present the full ambiguous, E- and B-mode decompositions discussed in Section 3.4 using the COSEBI-like statistics defined above. I also compute the Fisher information content of the approximate ambiguous, E- and B-mode subspaces for the parameters σ_8 and Ω_m . I use a basis composed of 50 correlation function bins logarithmically spaced from 1 to 400 arcmin. I find that the full basis composed of these different spaces completely spans the space of $2N$ data points, demonstrating that at least one such approximate decomposition exists.

Due to the fact that this decomposition is only approximate and that the matrices M_{\pm} are not exactly orthogonal for the vectors F_{\pm} , the different subspaces will in general not be perfectly orthog-

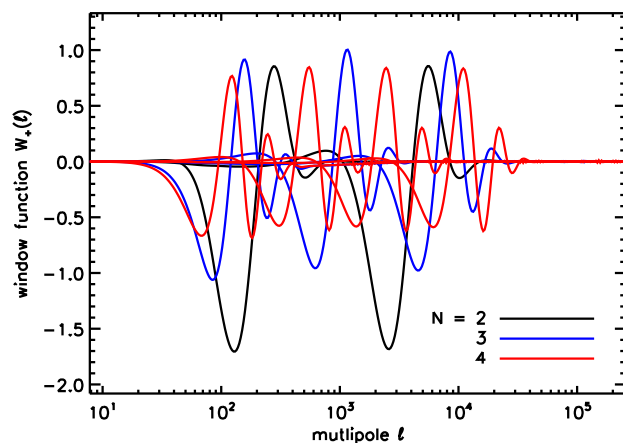


Figure 5. The Fourier space filters $W_+(\ell)$ for the $N \in \{2, 3, 4\}$ wavelet-like statistics computed for $\theta \in [1, 400]$ arcmin with 100 shear correlation function data points. The different colors show each of the filters. The $W_-(\ell)$ filters are approximately three orders of magnitude smaller than the $W_+(\ell)$ filters. The different filters in size (the overall width of the peaks and troughs) and location (the mean location in ℓ for each set of peaks and troughs) approximately cover all of ℓ -space accessible given the angular range of the data.

onal to one another. The degree of orthogonality of the ambiguous, E- and B-mode subspaces can be characterized by the maximum absolute normalized projection of a basis vector of any one of the spaces onto the basis vectors of the other spaces,

$$|\cos \theta| = \left| \frac{\vec{a} \cdot \vec{b}}{|\vec{a}| |\vec{b}|} \right| \quad (23)$$

where \vec{a} and \vec{b} are vectors of length $2N$ with the normal inner product definition. This quantity is just the cosine of the minimum angle between the vectors of any of the subspaces with the other. For subspaces which nearly share a basis vector, this maximum absolute normalized projection will be ≈ 1 , but it cannot be greater than one or else two of the vectors in the basis would be linearly dependent. For spaces which are mutually orthogonal, this maximum absolute normalized projection will be zero.

For the set of basis vectors just computed, I find that the maximum projection between the E- and B-mode subspaces is 1.39×10^{-1} . Similarly, the maximum projection between the E-mode and ambiguous subspaces is 1.51×10^{-3} and for the B-mode and ambiguous subspaces is 5.52×10^{-3} . Consistent with the argument made above, with equal area binning the E- and B-mode subspaces are more orthogonal with the maximum absolute normalized projection between them being 2.49×10^{-2} . However in this case, the ambiguous modes are less orthogonal to the E- and B-mode subspaces with the maximum absolute normalized projections being 1.31×10^{-1} and 3.19×10^{-1} respectively. The particularly poor orthogonality of the B-mode subspace to the ambiguous mode space in this case is reflected in the SVD of the matrix $M_+ M_-$ – I computed with equal area binning.

As mentioned above, the cost of E- and B-mode separation is that one must potentially throw away information in the ambiguous modes (e.g., Smith 2006; Schneider et al. 2010). Using the approximate mode decomposition described in this section, this point can be illustrated clearly and approached quantitatively. I compute the Fisher information content of the ambiguous, E- and B-mode sub-

spaces and combinations of them assuming Gaussian statistics and using the expressions presented above for the covariances of the two-point correlation functions and Fisher information matrices. For the E- and B-mode statistics, I simply transform the covariance matrix of the two-point correlation functions, since the statistics are linear combinations of the two-point data. One can obtain similar results computing their covariance matrices directly from their Fourier space window functions and the expressions presented in Section 3.5. The covariance matrix of the ambiguous modes is computed by direct transformation as well.

The Fisher information content $f \equiv \sqrt{|F|}$ of these subspaces for the parameters σ_8 and Ω_m using the binning scheme and angular range for the basis constructed above and also assuming DES-like errors is 2.18×10^4 , 3.49×10^4 , and 4.49×10^{-1} for the ambiguous, E- and B-mode subspaces respectively. By comparison, the full Fisher information for the entire two-point function data set, $\{\xi_{+i}, \xi_{-i}\}$ for $i \in [i, N]$, is 5.98×10^4 . Note that these figures are not additive and so can only be qualitatively compared. However the basic trends are clear. The B-mode subspace has very little information on the parameters as expected. Any residual information is either a numerical artifact or is due to E/B-mode mixing. The E-mode subspace has most of the information, but the ambiguous modes carry a non-trivial fraction of the total information. By retaining the ambiguous modes in the analysis with the E-modes, most of the information can be restored in comparison with the full two-point function with the E- plus ambiguous mode Fisher information being 5.75×10^4 . I have tested several other fiducial choices besides the COSEBI-like statistics for constructing the full mode decomposition of the correlation function data and found similar conclusions regarding the relative Fisher information content of the various subspaces. Similar conclusions hold for LSST-like surveys as well. While these Fisher information calculations are not particularly realistic as survey projections, they illustrate nicely the cost of E/B-mode separation in cosmic shear.

Finally, these Fisher information calculations can also illustrate the data compression properties of the COSEBI-like statistics. In particular, for the DES-like survey, the Fisher information in the first eight E-mode statistics is 3.46×10^4 as opposed to 3.49×10^4 for all of the E-mode statistics. Similarly, for the LSST-like survey using 100 correlation function bins in the same angular range as the DES-like survey, the first ten E-mode statistics have an information content of 6.489×10^5 as opposed to 6.496×10^5 for all of the E-mode statistics. These results are in qualitative agreement with those of Schneider et al. (2010).

5 CONCLUSIONS

In this work, I have demonstrated that the use of two-point E/B-mode estimators with binned shear correlation function data will generally result in non-trivial E/B-mode mixing. I computed the amount of this mixing and provided new E/B-mode estimators which minimize the unwanted mode mixing. I also gave practical recipes for building and using these estimators with binned cosmic shear data. Using these optimal estimators, I demonstrated that approximate decompositions of the vector space of binned correlation function points into ambiguous, E- and B-modes do exist. Using one of these decompositions, I found that the ambiguous mode subspace contains a non-trivial amount of information on typical cosmological parameters. I also gave two example applications of these new estimators to generic problems in cosmic shear data anal-

ysis, data compression (Section 4.1) and B-mode localization with wavelets (Section 4.2).

The estimators presented here have several nice features adapted to practical cosmic shear data analysis.

- They are linear combinations of the binned shear correlation function data, defined in Equation (2), and thus treat the binning explicitly. This property makes their computation and also error propagation/analysis with them trivial once the shear correlation function and its errors are known.
- The level of E/B-mode mixing due to the binning can be computed exactly, up to the knowledge of the binning window functions, for these estimators using Equations (7) and (8). In the limit of small bins, which is needed to suppress the E/B-mode mixing, the binning window functions are expected to be close to the geometric approximation used throughout this work.
- They give quantitative criteria in terms of the E/B-mode mixing by which to decide the number of shear correlation function bins to use, demonstrated in Figure 2 for the COSEBI-like estimators.
- The design of new E/B-mode estimators with specific purposes using the formalism presented in this work reduces to simple linear algebraic manipulations, presented in Section 3.2.

The optimal statistics presented in this work are well-suited to blinded or closed-box, high-precision cosmic shear data analyses. For example, before any shear correlation functions are computed from the data, one can estimate given the expected statistical accuracy of the data, the exact amount of E/B-mode mixing for a given binning scheme and set of estimators. One can then choose a fiducial binning scheme and estimator choice that properly minimizes the E/B-mode mixing and retains all of the cosmological information. Then these choices can be fixed throughout the data analysis process in order to avoid any observer biases in detecting or assessing B-mode contamination arising from how exactly the E/B-mode separation was done. Additionally, in a blinded or close-box analysis one might not look at plots of the shear correlation function data until the entire analysis is complete. Unfortunately in this case, one might miss crucial information about potential systematics in the *shape* of the shear correlation function data. The wavelet-like B-mode estimators presented in this work can be used as a substitute for and quantitative measure of the information gained by looking at the shape of the shear correlation function data. Additionally, they can be applied in automated way to large data sets in order to pinpoint areas of potential systematic contamination for further investigation. Importantly, because these estimators have a large degree of spatial locality, they can potentially provide crucial information on where any B-mode contamination is coming from and not just indicate its existence.

The ability to easily and quickly design E/B-mode estimators tailored to a specific purpose can potentially be very useful in practice as well. For instance, the problem of computing an E/B-mode statistic which maximizes the signal-to-noise or cosmological information content, as considered by Fu & Kilbinger (2010), could now be reformulated with the linear estimators presented here. Additionally, one could build estimators which are along the normal modes of the correlation function data computed from the correlation function covariance matrix. Also, one could attempt to build direct estimators for the E/B-mode correlation functions (Crittenden et al. 2002; Schneider et al. 2002b, 2010) over a finite interval. Alternatively, one could attempt to build filters which are localized in Fourier space in order to exclude certain wave modes, for example to mitigate the effects of uncertainty in the matter

power spectrum at small scales (see e.g., Huterer & White 2005), or to be sensitive to B-modes from only a range of ℓ . As simple linear combinations of cosmic shear data points, the estimators presented in this work are well-suited to these applications and to practical cosmic shear data analysis in general.

ACKNOWLEDGMENTS

I thank Tim Eifler, Eduardo Rozo, Scott Dodelson, Bhuvnesh Jain, Aaron Roodman, and the DES Weak Lensing Working Group for the many discussions which inspired aspects of this work. This work was supported by the Kavli Institute for Cosmological Physics at the University of Chicago through grants NSF PHY-0114422 and NSF PHY-0551142 and an endowment from the Kavli Foundation and its founder Fred Kavli. This work made extensive use of the NASA Astrophysics Data System and `arXiv.org` preprint server.

APPENDIX A: PAIR-WISE SHEAR CORRELATION FUNCTION ESTIMATORS AND FINITE BIN WIDTHS

I use the formalism presented in Appendix A of Schmidt et al. (2009) to derive the leading order bin weighting terms in the pair-wise estimator for the shear correlation functions. This estimator is (e.g., Schneider et al. 2002a)

$$\hat{\xi}_{\pm k} = \frac{\sum_{ij} w_i w_j W_{\theta_k}(x_i, x_j) (\epsilon_{it} \epsilon_{jt} \pm \epsilon_{i\times} \epsilon_{j\times})}{\sum_{ij} w_i w_j W_{\theta_k}(x_i, x_j)} \quad (\text{A1})$$

where $W_{\theta_k}(x_1, x_2)$ is the binning function which is unity inside the bin and zero outside with the bin centered at θ_k with some bin width $\Delta\theta$, $\epsilon_{it, i\times}$ is the component of the galaxy shape parallel or crossed with respect to the great circle connecting the two galaxies, and the $w_{i,j}$ are weights applied to each galaxy. Below I include the weights $w_{i,j}$ in the survey window function. Starting with Equation A15 of Schmidt et al. (2009) and assuming that the source galaxy density field is uncorrelated with the shear field and also neglecting lensing bias/reduced shear effects, the expectation value of this estimator can be written as

$$\begin{aligned} \langle \hat{\xi}_{ab} \rangle = & \frac{1}{\Omega_B} \int d^2 x_1 \int d^2 x_2 W_{\theta}(x_1, x_2) S(x_1) S(x_2) \\ & \times \xi_{ab}(|x_1 - x_2|) \left[1 + \xi_{gg}(|x_1 - x_2|) - \right. \\ & \left. \frac{1}{\Omega_B} \int d^2 x_3 \int d^2 x_4 W_{\theta}(x_3, x_4) S(x_1) S(x_2) \right. \\ & \left. \times \xi_{gg}(|x_3 - x_4|) \right] \quad (\text{A2}) \end{aligned}$$

where ξ_{ab} is the shear correlation function for $a, b \in \{t, \times\}$, $\Omega_B = \int d^2 x_1 \int d^2 x_2 W_{\theta}(x_1, x_2) S(x_1) S(x_2)$ is the survey averaged bin area, and ξ_{gg} is the source galaxy angular correlation function. $S(x_1)$ is the survey window function including the weights $w_{i,j}$. The second term in the brackets arises directly from the weighting over the bin by the sampling density of the source galaxies and the third term in the brackets is the first non-trivial term in the power-series expansion of the denominator of the estimator (i.e., the total number of observed galaxies in the bin). The last two terms in this integral do not exactly cancel as stated in Schmidt et al. (2009) because ξ_{gg} is not exactly equal to its average over the bin for all θ in the bin. In addition to this source clustering

weighting term, the survey window function contributes an additional weight over the bin. The form of this weighting function is highly non-trivial, but for small enough bins, this weighting should be negligible. However, quantitative results describing how small the bins need to be in order to suppress this weighting require detailed survey simulations, which are beyond the scope of this work. Thus for simplicity I neglect the survey window function weights. A simple estimate of the magnitude of the effect of source galaxy clustering using typical galaxy angular correlation functions (e.g., Connolly et al. 2002) shows that this effect (i.e., the difference of the last two terms in the bracket above) is $\lesssim 0.005$ when using at least five bins per decade. To get this number I assumed the galaxy-galaxy angular correlation function was a power law over the angular range of $[1, 400]$ arcmin with $\xi_{gg} = 0.0045 \times (\theta/1 \text{ deg})^{-0.7}$, consistent with the results of Connolly et al. (2002).

APPENDIX B: OPTIMAL E/B-MODE ESTIMATORS WITH GEOMETRIC BIN WEIGHTING FUNCTIONS

In this Appendix, I give the exact form of the constraint directions, F_{+a} and F_{+b} , and the matrix to compute the F_{-i} from the F_{+i} under the assumption of geometric bin weightings. Consider N bins in angle θ from L to H and let $[L_i, H_i]$ be the angular range of the i th bin. Also, assume the bins are non-overlapping. Then using the geometric bin weighting function, $W_i(\theta) = 2\theta/(H_i^2 - L_i^2)$, I get for the constraint direction vectors (see Section 3.2)

$$F_{+a} = (1, 1, 1, \dots, 1)_N \quad (\text{B1})$$

$$F_{+b} = \left(\frac{H_1^4 - L_1^4}{2(H_1^2 - L_1^2)}, \frac{H_2^4 - L_2^4}{2(H_2^2 - L_2^2)}, \frac{H_3^4 - L_3^4}{2(H_3^2 - L_3^2)}, \dots, \frac{H_N^4 - L_N^4}{2(H_N^2 - L_N^2)} \right)_N \quad (\text{B2})$$

The matrix to compute the F_{-k} in terms of the F_{+i} from Equation (12) is

$$(M_+)_{ki} = \delta_{ki} + \frac{2}{H_i^2 - L_i^2} \times \begin{cases} 2(H_i^2 - L_i^2) \ln(H_k/L_k) \\ \quad + \frac{3}{2}(H_i^4 - L_i^4) \left(\frac{1}{H_k^2} - \frac{1}{L_k^2} \right) & \text{if } i < k \\ -\frac{1}{2}(H_k^2 - L_k^2) - 2L_i^2 \ln(H_k/L_k) \\ \quad - \frac{3}{2}L_i^4 \left(\frac{1}{H_k^2} - \frac{1}{L_k^2} \right) & \text{if } i = k \\ 0 & \text{if } i > k \end{cases} \quad (\text{B3})$$

where i and k run over 1 to N . Then the F_{-k} are computed as

$$F_{-k} = \sum_{i=1}^N (M_+)_{ki} F_{+i} \quad (\text{B4})$$

APPENDIX C: OPTIMAL E/B-MODE ESTIMATORS WITH F_- FIXED

One can easily define optimal E/B-mode estimators with F_- fixed instead of F_+ fixed. In this case one fixes the F_+ by minimizing

$$0 = \frac{\partial}{\partial F_{+k}} \left[\int_0^\infty d\ell \ell |W_-(\ell)|^2 \right] \quad (\text{C1})$$

The solution to this equation is (c.f. Equation 12)

$$F_{+k} = F_{-k} + \left(\int_{L_k}^{H_k} d\theta \frac{W_k^2(\theta)}{\theta} \right)^{-1} \sum_i F_{-i} \\ \times \int_{L_i}^{H_i} \int_{L_k}^{H_k} d\theta d\phi W_i(\theta) W_k(\phi) \\ \times \left(\frac{4}{\theta^2} - \frac{12\phi^2}{\theta^4} \right) H(\theta - \phi). \quad (\text{C2})$$

In this case the constraint directions can be derived by similar arguments to the those in Section 3.2 and are

$$F_{-a} = \left(\int_{L_1}^{H_1} d\theta \frac{W_1(\theta)}{\theta^2}, \int_{L_2}^{H_2} d\theta \frac{W_2(\theta)}{\theta^2}, \dots, \int_{L_N}^{H_N} d\theta \frac{W_N(\theta)}{\theta^2} \right)_N \quad (\text{C3})$$

$$F_{-b} = \left(\int_{L_1}^{H_1} d\theta \frac{W_1(\theta)}{\theta^4}, \int_{L_2}^{H_2} d\theta \frac{W_2(\theta)}{\theta^4}, \dots, \int_{L_N}^{H_N} d\theta \frac{W_N(\theta)}{\theta^4} \right)_N \quad (\text{C4})$$

and Equation (C2) again defines a matrix which is used to compute the F_+ in terms of the F_- . Finally, for the geometric bin weighting functions the constraint directions and matrix relating the F_+ to F_- are

$$F_{-a} = \left(\frac{2 \log[H_1/L_1]}{H_1^2 - L_1^2}, \frac{2 \log[H_2/L_2]}{H_2^2 - L_2^2}, \dots, \frac{2 \log[H_N/L_N]}{H_N^2 - L_N^2} \right)_N \quad (\text{C5})$$

$$F_{-b} = \left(\frac{1}{H_1^2 - L_1^2} \left(\frac{1}{L_1^2} - \frac{1}{H_1^2} \right), \frac{1}{H_2^2 - L_2^2} \left(\frac{1}{L_2^2} - \frac{1}{H_2^2} \right), \dots, \frac{1}{H_N^2 - L_N^2} \left(\frac{1}{L_N^2} - \frac{1}{H_N^2} \right) \right)_N \quad (\text{C6})$$

and

$$(M_-)_{ki} = \delta_{ki} + \frac{2}{H_i^2 - L_i^2} \\ \times \begin{cases} 0 & \text{if } i < k \\ \frac{1}{2} \left[-H_k^2 + L_k^2 (4 - 3L_k^2/H_i^2) - 4 \ln(H_i/L_k) \right] & \text{if } i = k \\ 2(H_k^2 - L_k^2) \ln(H_i/L_i) + \frac{3}{2} (H_k^4 - L_k^4) \left(\frac{1}{H_i^2} - \frac{1}{L_i^2} \right) & \text{if } i > k \end{cases} \quad (\text{C7})$$

where i and k run over 1 to N . Then the F_{+k} are computed as

$$F_{+k} = \sum_{i=1}^N (M_-)_{ki} F_{-i}. \quad (\text{C8})$$

REFERENCES

Antonik M. L. et al., 2012, arXiv:astro-ph/1206.5320
 Bartelmann M., 2010, *Class. Quant. Grav.*, 27, 233001
 Bartelmann M., Schneider P., 2001, *Phys. Rep.*, 340, 291
 Bernardeau F., Bonvin C., Vernizzi F., 2010, *Phys. Rev. D*, 81, 083002

Bernstein G., Huterer D., 2010, *MNRAS*, 401, 1399
 Bernstein G. M., Jarvis M., 2002, *AJ*, 123, 583
 Beynon E., Bacon D. J., Koyama K., 2010, *MNRAS*, 403, 353
 Bridle S. et al., 2010, *MNRAS*, 405, 2044
 Bridle S., King L., 2007, *New Journal of Physics*, 9, 444
 Casarini L., Bonometto S. A., Borgani S., Dolag K., Murante G., Mezzetti M., Tornatore L., La Vacca G., 2012, *A&A*, 542, A126
 Casarini L., Macciò A. V., Bonometto S. A., Stinson G. S., 2011, *MNRAS*, 412, 911
 Catelan P., Kamionkowski M., Blandford R. D., 2001, *MNRAS*, 320, L7
 Connolly A. J. et al., 2002, *ApJ*, 579, 42
 Cooray A., Hu W., 2002, *ApJ*, 574, 19
 Cooray A. R., 1999, *A&A*, 348, 31
 Crittenden R. G., Natarajan P., Pen U.-L., Theuns T., 2001, *ApJ*, 559, 552
 Crittenden R. G., Natarajan P., Pen U.-L., Theuns T., 2002, *ApJ*, 568, 20
 Croft R. A. C., Metzler C. A., 2000, *ApJ*, 545, 561
 Cunha C. E., Huterer D., Busha M. T., Wechsler R. H., 2012, *MNRAS*, 423, 909
 Cypriano E. S., Amara A., Voigt L. M., Bridle S. L., Abdalla F. B., Réfrégier A., Seiffert M., Rhodes J., 2010, *MNRAS*, 405, 494
 de Bernardis F., Kitching T. D., Heavens A., Melchiorri A., 2009, *Phys. Rev. D*, 80, 123509
 Debono I., Rassat A., Réfrégier A., Amara A., Kitching T. D., 2010, *Annalen der Physik*, 522, 324
 Dodelson S., 2003, *Modern cosmology*. Amsterdam (Netherlands): Academic Press
 Eifler T., Schneider P., Krause E., 2010, *A&A*, 510, A7
 Eisenstein D. J., Hu W., 1998, *ApJ*, 496, 605
 Fedeli C., Moscardini L., 2010, *MNRAS*, 405, 681
 Fu L., Kilbinger M., 2010, *MNRAS*, 401, 1264
 Fu L. et al., 2008, *A&A*, 479, 9
 Giannantonio T., Porciani C., Carron J., Amara A., Pillepich A., 2012, *MNRAS*, 422, 2854
 Guillet T., Teyssier R., Colombi S., 2010, *MNRAS*, 405, 525
 Guzik J., Bernstein G., 2005, *Phys. Rev. D*, 72, 043503
 Hahn O., Teyssier R., Carollo C. M., 2010, *MNRAS*, 405, 274
 Hannestad S., Tu H., Wong Y. Y., 2006, *Journal of Cosmology and Astro-Particle Physics*, 6, 25
 Harnois-Deraps J., Vafaei S., Van Waerbeke L., 2012, arXiv:astro-ph/1202.2332
 Hearin A. P., Zentner A. R., 2009, *Journal of Cosmology and Astro-Particle Physics*, 4, 32
 Hearin A. P., Zentner A. R., Ma Z., 2012, *Journal of Cosmology and Astro-Particle Physics*, 4, 34
 Hearin A. P., Zentner A. R., Ma Z., Huterer D., 2010, *ApJ*, 720, 1351
 Heavens A., 2003, *MNRAS*, 343, 1327
 Heavens A., Refregier A., Heymans C., 2000, *MNRAS*, 319, 649
 Heymans C. et al., 2006a, *MNRAS*, 368, 1323
 Heymans C., White M., Heavens A., Vale C., van Waerbeke L., 2006b, *MNRAS*, 371, 750
 Hikage C., Takada M., Hamana T., Spergel D., 2011, *MNRAS*, 412, 65
 Hilbert S., Hartlap J., White S. D. M., Schneider P., 2009, *A&A*, 499, 31
 Hilbert S., Marian L., Smith R. E., Desjacques V., 2012, arXiv:astro-ph/1204.4530
 Hirata C., Seljak U., 2003, *MNRAS*, 343, 459

- Hirata C. M., Mandelbaum R., Ishak M., Seljak U., Nichol R., Pimbblet K. A., Ross N. P., Wake D., 2007, *MNRAS*, 381, 1197
- Hirata C. M., Seljak U., 2004, *Phys. Rev. D*, 70, 063526
- Hoekstra H., 2004, *MNRAS*, 347, 1337
- Hoekstra H., Jain B., 2008, *Annual Review of Nuclear and Particle Science*, 58, 99
- Hu W., White M., 2001, *ApJ*, 554, 67
- Hui L., Zhang J., 2008, *ApJ*, 688, 742
- Huterer D., Takada M., 2005, *Astroparticle Physics*, 23, 369
- Huterer D., Takada M., Bernstein G., Jain B., 2006, *MNRAS*, 366, 101
- Huterer D., White M., 2005, *Phys. Rev. D*, 72, 043002
- Ichiki K., Takada M., Takahashi T., 2009, *Phys. Rev. D*, 79, 023520
- Jain B., Seljak U., White S., 2000, *ApJ*, 530, 547
- Jarvis M., Bernstein G., Jain B., 2004, *MNRAS*, 352, 338
- Jarvis M., Jain B., 2004, *arXiv:astro-ph/0412234*
- Jimenez R., Kitching T., Peña-Garay C., Verde L., 2010, *Journal of Cosmology and Astro-Particle Physics*, 5, 35
- Jing Y. P., 2002, *MNRAS*, 335, L89
- Jing Y. P., Zhang P., Lin W. P., Gao L., Springel V., 2006, *ApJ*, 640, L119
- Joachimi B., Schneider P., Eifler T., 2008, *A&A*, 477, 43
- Kacprzak T., Zuntz J., Rowe B., Bridle S., Refregier A., Amara A., Voigt L., Hirsch M., 2012, *arXiv:astro-ph/1203.5049*
- Kaiser N., 1992, *ApJ*, 388, 272
- Kaiser N., 2000, *ApJ*, 537, 555
- Kiessling A., Heavens A. F., Taylor A. N., Joachimi B., 2011, *MNRAS*, 414, 2235
- Kilbinger M., Munshi D., 2006, *MNRAS*, 366, 983
- Kilbinger M., Schneider P., Eifler T., 2006, *A&A*, 457, 15
- Kirk D., Rassat A., Host O., Bridle S., 2012, *MNRAS*, 3339
- Kitching T. D. et al., 2012, *MNRAS*, 3181
- Kitching T. D., Heavens A. F., Verde L., Serra P., Melchiorri A., 2008, *Phys. Rev. D*, 77, 103008
- Krause E., Hirata C. M., 2010, *A&A*, 523, A28
- Krause E., Schneider P., Eifler T., 2012, *MNRAS*, 3177
- Laszlo I., Bean R., Kirk D., Bridle S., 2012, *MNRAS*, 423, 1750
- Lee J., Pen U.-L., 2002, *ApJ*, 567, L111
- Lee J., Pen U.-L., 2008, *ApJ*, 681, 798
- Leonard A., Pires S., Starck J.-L., 2012, *MNRAS*, 423, 3405
- Lin H. et al., 2011, *arXiv:astro-ph/1111.6622*
- Ma Z., Hu W., Huterer D., 2006, *ApJ*, 636, 21
- Mandelbaum R., Hirata C. M., Ishak M., Seljak U., Brinkmann J., 2006a, *MNRAS*, 367, 611
- Mandelbaum R., Seljak U., Cool R. J., Blanton M., Hirata C. M., Brinkmann J., 2006b, *MNRAS*, 372, 758
- Marian L., Hilbert S., Smith R. E., Schneider P., Desjacques V., 2011, *ApJ*, 728, L13
- Markovic K., Bridle S., Slosar A., Weller J., 2011, *Journal of Cosmology and Astro-Particle Physics*, 1, 22
- Massey R. et al., 2007, *MNRAS*, 376, 13
- Maturi M., Fedeli C., Moscardini L., 2011, *MNRAS*, 416, 2527
- Paulin-Henriksson S., Amara A., Voigt L., Refregier A., Bridle S. L., 2008, *A&A*, 484, 67
- Press W. H., Teukolsky S. A., Vetterling W. T., Flannery B. P., 1992, *Numerical Recipes in C*, 2nd edn. Cambridge (United Kingdom): Cambridge University Press
- Refregier A., Kacprzak T., Amara A., Bridle S., Rowe B., 2012, *arXiv:astro-ph/1203.5050*
- Ricker N., 1953, *Geophysics*, 18, 10
- Rudd D. H., Zentner A. R., Kravtsov A. V., 2008, *ApJ*, 672, 19
- Sato M., Hamana T., Takahashi R., Takada M., Yoshida N., Matsumura T., Sugiyama N., 2009, *ApJ*, 701, 945
- Schaefer B. M., Caldera-Cabral G. A., Maartens R., 2008, *arXiv:astro-ph/0803.2154*
- Schmidt F., 2008, *Phys. Rev. D*, 78, 043002
- Schmidt F., Rozo E., Dodelson S., Hui L., Sheldon E., 2009, *ApJ*, 702, 593
- Schneider P., Eifler T., Krause E., 2010, *A&A*, 520, A116
- Schneider P., Kilbinger M., 2007, *A&A*, 462, 841
- Schneider P., Kilbinger M., Lombardi M., 2005, *A&A*, 431, 9
- Schneider P., Seitz C., 1995, *A&A*, 294, 411
- Schneider P., van Waerbeke L., Jain B., Kruse G., 1998, *MNRAS*, 296, 873
- Schneider P., van Waerbeke L., Kilbinger M., Mellier Y., 2002a, *A&A*, 396, 1
- Schneider P., van Waerbeke L., Mellier Y., 2002b, *A&A*, 389, 729
- Seljak U., 1998, *ApJ*, 506, 64
- Semboloni E., Heymans C., van Waerbeke L., Schneider P., 2008, *MNRAS*, 388, 991
- Semboloni E., Tereno I., van Waerbeke L., Heymans C., 2009, *MNRAS*, 397, 608
- Shi X., Schneider P., Joachimi B., 2011, *A&A*, 533, A48
- Smith K. M., 2006, *Phys. Rev. D*, 74, 083002
- Smith R. E. et al., 2003, *MNRAS*, 341, 1311
- Song Y.-S., Knox L., 2004, *Phys. Rev. D*, 70, 063510
- Sun L., Fan Z.-H., Tao C., Kneib J.-P., Jovel S., Tilquin A., 2009, *ApJ*, 699, 958
- Tegmark M., Taylor A. N., Heavens A. F., 1997, *ApJ*, 480, 22
- Teyssier R. et al., 2009, *A&A*, 497, 335
- Vale C., Hoekstra H., van Waerbeke L., White M., 2004, *ApJ*, 613, L1
- Vale C., White M., 2003, *ApJ*, 592, 699
- van Daalen M. P., Schaye J., Booth C. M., Dalla Vecchia C., 2011, *MNRAS*, 415, 3649
- Vanderveld R. A., Caldwell R. R., Rhodes J., 2011, *Phys. Rev. D*, 84, 123510
- Voigt L. M., Bridle S. L., 2010, *MNRAS*, 404, 458
- Voigt L. M., Bridle S. L., Amara A., Cropper M., Kitching T. D., Massey R., Rhodes J., Schrabback T., 2012, *MNRAS*, 421, 1385
- Wandelt B. D., Hivon E., Górski K. M., 2001, *Phys. Rev. D*, 64, 083003
- Weinberg D. H., Mortonson M. J., Eisenstein D. J., Hirata C., Riess A. G., Rozo E., 2012, *arXiv:astro-ph/1201.2434*
- White M., 2004, *Astroparticle Physics*, 22, 211
- Zhan H., Knox L., 2004, *ApJ*, 616, L75

This paper has been typeset from a \LaTeX file prepared by the author.